

Object-Centric Domain Randomization for 3D Shape Reconstruction in the Wild

Junhyeong Cho¹ Kim Youwang² Hunmin Yang^{1,4} Tae-Hyun Oh^{2,3,5}

¹ADD ²Department of EE, POSTECH ³Graduate School of AI, POSTECH ⁴KAIST
⁵Institute for Convergence Research and Education in Advanced Technology, Yonsei University
<https://ObjectDR.github.io>

Abstract. One of the biggest challenges in single-view 3D shape reconstruction in the wild is the scarcity of (3D shape, 2D image)-paired data from real-world environments. Inspired by remarkable achievements via domain randomization, we propose *ObjectDR* which synthesizes such paired data via a random simulation of visual variations in object appearances and backgrounds. Our data synthesis framework exploits a conditional generative model (*e.g.*, ControlNet) to generate images conforming to spatial conditions such as 2.5D sketches, which are obtainable through a rendering process of 3D shapes from object collections (*e.g.*, Objaverse-XL). To simulate diverse variations while preserving object silhouettes embedded in spatial conditions, we also introduce a disentangled framework which leverages an initial object guidance. After synthesizing a wide range of data, we pre-train a model on them so that it learns to capture a domain-invariant geometry prior which is consistent across various domains. We validate its effectiveness by substantially improving 3D shape reconstruction models on a real-world benchmark. In a scale-up evaluation, our pre-training achieves 23.6% superior results compared with the pre-training on high-quality computer graphics renderings.

Keywords: domain randomization · 3D shape reconstruction · data synthesis

1 Introduction

The abundance of large-scale data [15, 39, 68–70] has been the driving force behind recent breakthroughs in computer vision tasks [8, 35, 44, 47, 62, 67]. However, there remains a shortage of real-world (3D shape, 2D image)-paired data; it is nearly infeasible to precisely acquire large-scale 3D shape annotations in real scenes due to its substantial cost. Owing to the scarcity of data collected from real-world environments, single-view 3D shape reconstruction in the wild still remains an ongoing challenge.

In this paper, we argue that conditional generative models [45, 56, 61, 90] could shed light on this challenge by synthesizing large-scale (3D shape, 2D image)-paired data. Such generative models are capable of synthesizing realistic images that conform to spatial conditions such as 2.5D sketches (*e.g.*, depth maps). Since 2.5D sketches are obtainable through a rendering process of 3D objects, we could generate various images from 3D objects via the generative models (see Fig. 1). Considering a substantial amount of 3D objects [9, 12, 15, 48], we raised a question “*Could we empower 3D perception capable of recognizing 3D shapes appeared in diverse real-world environments via a large-scale random simulation powered by the prior of generative models?*”

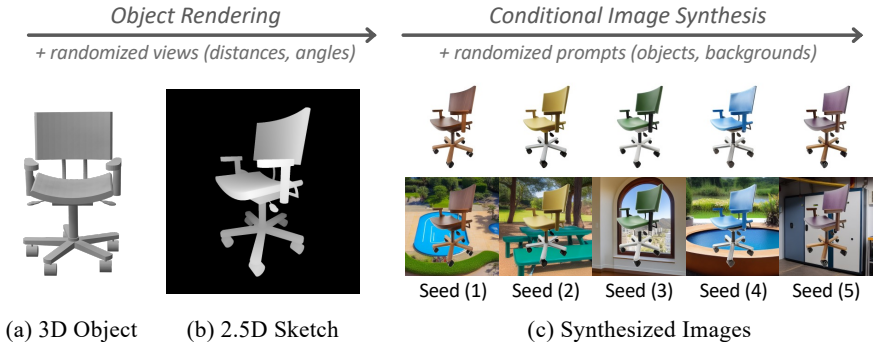


Fig. 1: Overview of the proposed data synthesis framework. From a 3D object, we acquire its 2.5D sketch (e.g., depth map) through a rendering process. Then, a conditional generative model (e.g., ControlNet [90]) synthesizes diverse images using the 2.5D sketch and randomized prompts. By setting random seeds, we simulate random visual variations in object appearances and backgrounds. We pre-train a 3D shape reconstruction model on such randomized data so that it learns to capture a domain-invariant geometry prior which is consistent across various environments.

We propose a scalable data synthesis framework, called **ObjectDR (Object-Centric Domain Randomization)**, which aims to simulate a wide range of random visual variations. By pre-training a 3D shape reconstruction model on our synthesized data, we expose the model to diverse variations in object appearances and backgrounds. In this way, the model learns to capture a domain-invariant geometry prior that is consistent across domains, facilitating its generalization across diverse environments. By exposing the model to random occlusions during the model pre-training, we also improve its resilience against occlusions commonly encountered in real-world environments.

The effectiveness of ObjectDR depends on *diversity* and *fidelity* of synthesized data. In this paper, *diversity* indicates the variety of visual variations in object appearances and backgrounds, whereas *fidelity* denotes how precisely conditional generative models comply with input spatial conditions. Note that *fidelity* determines whether we could regard the used 3D objects as ground-truth 3D shapes for objects featured in synthesized images. As shown in Fig. 2, we observed that these two factors appear as a trade-off relationship when exploiting pre-trained conditional generative models [45, 56, 61, 90]. When the conditional generative models are enforced to precisely follow the input spatial conditions, they produce monotonous backgrounds due to the lack of background information in the conditions. On the other hand, if we encourage such models to diversify backgrounds using textual conditions, they tend to generate various backgrounds at the expense of violating the input spatial conditions.

To effectively deal with the trade-off relationship, we propose **ObjectDR_{dis}** which disentangles the randomization process of object appearances and backgrounds. The proposed framework randomizes object appearances and backgrounds in a separate manner, and then integrates them. Using this disentangled framework, we leverage an initial object guidance which significantly improves the fidelity at the expense of monotonous backgrounds. In parallel, we also enhance the diversity of backgrounds by synthesizing random authentic scenes without being constrained by objects.



Fig. 2: Trade-off relationship between diversity and fidelity observed from pre-trained conditional generative models [45, 56, 61, 90]. When we use 2.5D sketches rendered from 3D objects, background synthesis leads to the violation of spatial conditions. We highlight regions with red circles.

We demonstrate the proposed data synthesis framework using ControlNet [90] with a variety of 3D objects from Objaverse-XL [15], MeshDiffusion [48], ShapeNet [9] and ABO [12]. We validate the effectiveness of our framework by pre-training AtlasNet [31] and Mesh R-CNN [28] on our synthesized 110.8K $\langle 3D \text{ shape}, 2D \text{ image} \rangle$ -paired data. The results show that the model pre-training significantly improves their accuracies on a real-world benchmark [75]. Also, this pre-training leads to 23.6% better results than the pre-training on high-quality computer graphics renderings in a scale-up evaluation.

Our main contributions are summarized as follows:

- We propose ObjectDR which synthesizes $\langle 3D \text{ shape}, 2D \text{ image} \rangle$ -paired data in a scalable manner via a random simulation of object appearances and backgrounds.
- We propose ObjectDR_{dis} which effectively tackles the diversity-fidelity trade-off observed from pre-trained generative models via a disentangled framework.
- We construct a large-scale dataset which consists of diverse and high-fidelity 110.8K $\langle 3D \text{ shape}, 2D \text{ image} \rangle$ -paired data generated by the proposed random simulation.
- The proposed pre-training substantially improves 3D shape reconstruction models on a real-world benchmark. In a scale-up evaluation, it achieves 23.6% superior results compared with the pre-training on high-quality computer graphics renderings.

2 Related Work

Single-view 3D shape reconstruction in the wild. This task aims to estimate a 3D shape from a single image captured in a real-world environment. It is challenging because real-world objects exhibit a variety of shapes while their appearances are greatly altered by environmental factors (*e.g.*, lighting conditions). To handle such variations, 3D shape estimation models [1, 11, 25, 27–29, 31, 34, 46, 55, 58, 59, 78, 80, 83–85, 89, 92] should generalize well across different environments. However, the scarcity of real-world $\langle 3D \text{ shape}, 2D \text{ image} \rangle$ -paired data poses a significant obstacle in the pursuit of the goal.

In this paper, we address this issue using a random simulation for the synthesis of large-scale $\langle 3D \text{ shape}, 2D \text{ image} \rangle$ -paired data. Our approach could generate an infinite number of diverse images using conditional generative models [45, 56, 61, 90] with a substantial amount of 3D shapes from object collections [9, 12, 15, 16, 40] or generative models [10, 48, 72, 84]. Given that the widely used real-world dataset [75] contains only 10K images, this approach might lead to a significant advance in this research field.

Table 1: Comparison of assets required for the diversification of object appearances and backgrounds. By leveraging the prior of generative models, our approach does not require texture maps and environment maps. In contrast, CG tools need such additional assets for the diversification.

Data Synthesis	# Texture Maps	# Environment Maps	Diversity
Computer Graphics	P	Q	$\propto PQ$
ObjectDR (Ours)	0	0	∞

Synthetic data generation. Several computer vision tasks are often framed as inverse graphics, and there have been natural attempts [1–5, 17, 18, 22, 23, 26, 30, 32, 36, 52, 63, 66, 74, 78, 82, 87] to exploit synthetic datasets obtained through forward computer graphics (CG) pipelines, *i.e.*, rendering. They have demonstrated successes in many computer vision tasks including 3D human and animal estimation, where acquiring precise annotations from data captured in real-world environments is challenging.

For 3D shape reconstruction, we could also synthesize data by rendering 3D objects from object collections (*e.g.*, Objaverse-XL [15], ShapeNet [9], ABO [12]) via CG tools. As long as sufficient 3D shapes and texture assets are available for objects and environments, this approach could facilitate 3D shape reconstruction in the wild. However, it is expensive to collect a great variety of high-quality assets (*e.g.*, 4K-resolution texture maps, HDRI maps) needed to bridge the gap between synthetic and real-world environments. Furthermore, the diversity of object appearances and backgrounds depicted by rendered images is determined by the combination of available assets (see Table 1).

Compared with CG tools, the proposed data synthesis framework could randomly simulate an infinite number of object appearances and backgrounds without using such additional assets. Instead of the high-quality assets, our approach leverages the prior of generative models pre-trained on a great variety of real-world images. Since state-of-the-art generative models [45, 56, 61, 67, 90] are publicly available, this approach could enable a more scalable synthesis of {3D shape, 2D image}-paired data.

Improving model robustness to distribution shifts. To enhance the model robustness, it is common to exploit multiple domains for learning domain-invariant features [7, 19, 37, 41, 43, 50, 51, 71, 94, 95]. However, acquiring multiple domains from real-world environments might be infeasible in several cases. To effectively deal with this issue, domain randomization methods [14, 21, 33, 53, 60, 65, 76, 77, 88] synthesize multiple domains via a random simulation of diverse scenarios. By exposing a model to such randomized variations, the model learns to capture generalizable representations capable of handling a wide range of variations encountered in real-world scenarios.

Following the paradigm of domain randomization, we simulate random visual variations in object appearances and backgrounds to effectively tackle a wide range of real-world objects and environments. Although randomized data may have physically implausible compositions (*e.g.*, a chair hovering in the sky), they could cover more extreme distribution shifts. We argue that such data would be useful for improving model’s robustness in line with the core idea of domain randomization methods. By pre-training a 3D shape reconstruction model on such randomized data, the model learns to capture a domain-invariant geometry prior useful for handling diverse visual variations caused by a variety of factors in real-world environments.

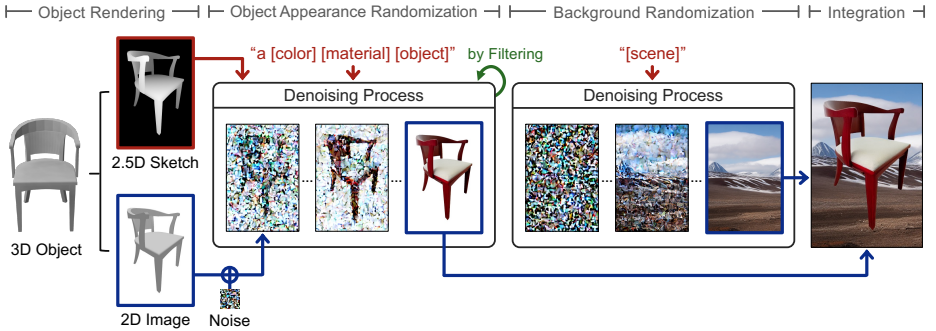


Fig. 3: Overall framework of ObjectDR_{dis}. Firstly, we render a 3D object to obtain a 2.5D sketch and an image. Then, we simulate random object appearances via a conditional diffusion model using the 2.5D sketch as its spatial condition and “a [color] [material] [object]” (e.g., “a red wood chair”) as its textual condition; [color] and [material] are randomly selected from word collections, while [object] denotes the category of the used 3D object. To achieve high fidelity, we utilize the rendered image as an initial object guidance and filter inadequate images. In a separate manner, we simulate random backgrounds via a generative model using “[scene]” (e.g., “tundra”) as its textual condition; [scene] is randomly selected from extensive scene categories. Then, we integrate the object and background images via an object silhouette mask obtainable from the 2.5D sketch.

3 Method

The overall framework of ObjectDR_{dis} is illustrated in Fig. 3 and elaborated in Alg. 1. In this section, we introduce the process of object rendering (Sec. 3.1), random simulation of object appearances (Sec. 3.2) and random simulation of backgrounds (Sec. 3.3). After synthesizing object appearances and backgrounds, we integrate them via object silhouette masks obtainable from 2.5D sketches.

Goal. The proposed framework aims at simulating random visual variations in object appearances and backgrounds to facilitate 3D shape reconstruction in the wild. By pre-training a model on such randomized data, the model learns to capture a domain-invariant geometry prior that is consistent across diverse environments. To further improve its robustness, we also simulate random occlusions during the model pre-training.

3.1 Object Rendering

3D shape collections [9, 12, 15] provide a great variety of 3D objects. For example, Objaverse-XL [15] contains more than 10 million 3D objects. In addition to them, we could also synthesize 3D objects using generative models such as MeshDiffusion [48]. By utilizing them, we obtain a substantial number of K objects for ObjectDR_{dis}.

Given a 3D object, we render it using N camera views constructed by random variations in camera distances with random elevation and azimuth angles. From each camera view, we obtain a 2.5D sketch (e.g., depth map) and an image. The 2.5D sketch is used as a spatial condition for synthesizing object images, and the rendered image is used as an initial object guidance. As shown in Alg. 1, the 2.5D sketch is also used to extract an object silhouette mask.

Algorithm 1 ObjectDR_{dis}

Requirement: object renderer $\mathcal{R}(\cdot)$, guidance perturber $\mathcal{P}(\cdot)$, random seed generator $\mathcal{G}(\cdot)$, conditional diffusion model $\mathcal{D}_1(\cdot)$, conditional diffusion model $\mathcal{D}_2(\cdot)$

Input: 3D objects $\{\mathcal{O}_i\}_{i=1}^K$, number of views N , number of synthesis per 2.5D sketch M , color collection \mathcal{C}_c , material collection \mathcal{C}_m , scene collection \mathcal{C}_s , filtering threshold τ

Output: KNM (3D shape, 2D image)-paired data

```

1:  $\{2.5D_{i,j}\}_{i=1,j=1}^{K,N}, \{2D_{i,j}\}_{i=1,j=1}^{K,N} \leftarrow \mathcal{R}(\{\mathcal{O}_i\}_{i=1}^K, N)$   $\triangleright$  render  $K$  objects using  $N$  views
2:  $\{\text{mask}_{i,j}\}_{i=1,j=1}^{K,N} \leftarrow \text{extract\_mask}(\{2.5D_{i,j}\}_{i=1,j=1}^{K,N})$   $\triangleright$  extract object silhouette masks
3: output  $\leftarrow []$ 
4: for  $i = 1, 2, \dots, K$  do
5:   for  $j = 1, 2, \dots, N$  do
6:     for  $\text{iteration} = 1, 2, \dots, M$  do  $\triangleright$  synthesize  $M$  images per 2.5D $i,j$ 
7:       guide  $\leftarrow \mathcal{P}(2D_{i,j})$   $\triangleright$  perturb an initial guidance
8:       while True do
9:         seed  $\leftarrow \mathcal{G}()$   $\triangleright$  set random seed
10:        [color], [material]  $\leftarrow \text{sample}(\mathcal{C}_c, \mathcal{C}_m, \text{seed})$   $\triangleright$  randomly select words
11:        [object]  $\leftarrow \text{retrieve\_category}(\mathcal{O}_i)$   $\triangleright$  retrieve 3D object category
12:        txt  $\leftarrow$  "a [color] [material] [object]"
13:        obj  $\leftarrow \mathcal{D}_1(2.5D_{i,j}, \text{guide}, \text{txt}, \text{seed})$   $\triangleright$  simulate object appearance
14:        if not is_filtered(obj, mask $i,j$ ,  $\tau$ ) then  $\triangleright$  filter an image with  $\tau$ 
15:          break
16:        end if
17:      end while
18:      seed  $\leftarrow \mathcal{G}()$   $\triangleright$  set random seed
19:      [scene]  $\leftarrow \text{sample}(\mathcal{C}_s, \text{seed})$   $\triangleright$  randomly select a word
20:      txt  $\leftarrow$  "[scene]"
21:      bg  $\leftarrow \mathcal{D}_2(\text{txt}, \text{seed})$   $\triangleright$  simulate background
22:      img  $\leftarrow \text{integrate}(\text{obj}, \text{bg}, \text{mask}_{i,j})$   $\triangleright$  integrate obj and bg via mask $i,j$ 
23:      Add ( $\mathcal{O}_i$ , img) to output
24:    end for
25:  end for
26: end for
27: return output

```

3.2 Object Appearance Randomization

To simulate random visual variations in object appearances, we leverage the prior of a pre-trained conditional diffusion model (e.g., ControlNet [90]). Since the model has already seen a considerable number of real-world images, it could synthesize diverse yet realistic object appearances. In our framework, the generative model simulates various variations with different random seeds using 2.5D sketch as its spatial condition and "a [color] [material] [object]" as its textual condition. Note that [color] and [material] are randomly selected from color collection \mathcal{C}_c and material collection \mathcal{C}_m , while [object] denotes the category of the used 3D object. To simulate more diverse appearances, we could also randomize the text template by simply adding an empty string to the collections. In this case, the model synthesizes random appearances using these templates: "a [color] [material] [object]", "a [color] [object]", "a [material] [object]", and "a [object]".

Initial object guidance. Such a conditional diffusion model occasionally distorts the spatial structure depicted in the input spatial condition. However, we should preserve the exact spatial structure to regard the used 3D objects as the ground-truth 3D shapes for objects featured in synthesized images. To improve fidelity, we additionally exploit the rendered image as an initial object guidance. Motivated by SDEdit [54], we perturb the initial guidance with Gaussian noise and feed it to the diffusion model. Since the noisy guidance still preserves its original spatial structure, the conditional diffusion model could focus on randomizing object appearances without distorting the spatial structure while progressively removing the noise. We observe that the initial guidance is effective for enhancing fidelity in our empirical experiments.

Filtering synthesized images. Although the initial guidance substantially improves fidelity in most cases, minor disparities may still be observable between mask-depicted silhouettes and the actual foreground silhouettes in synthesized images. Thus, we filter images if the intersection-over-union (IoU) values between those silhouettes are less than τ . Note that it is important to precisely acquire the actual silhouettes for the effective filtering. By leveraging the initial guidance which leads to nearly-white backgrounds in synthesized images, we could easily extract foreground objects using a threshold.

3.3 Background Randomization

To simulate diverse backgrounds, one could randomly select a scene image from scene datasets such as SUN [86] and Places365 [93]. However, it substantially limits the diversity of backgrounds by the coverage of scene images included in the selected datasets. Instead of this approach, we leverage the prior of a conditional generative model pre-trained on a significantly larger number of images.

Such a conditional generative model could effectively synthesize random authentic scenes with different random seeds using “[scene]” as its textual condition, where [scene] indicates a scene category randomly selected from scene collection \mathcal{C}_s . To simulate a great variety of backgrounds, we could build the collection \mathcal{C}_s by exploiting extensive scene categories from scene recognition datasets [86, 93].

4 Experiments

In this section, we analyze the proposed data synthesis framework (Sec. 4.1), generate ⟨3D shape, 2D image⟩-paired data for model pre-training (Sec. 4.2), and validate the effectiveness of our randomized data with AtlasNet [31] (Sec. 4.3) and Mesh R-CNN [28] (Sec. 4.4). Please refer to the supplementary material for more details and results.

Implementation details. We use a great variety of 3D objects from Objaverse-XL [15], MeshDiffusion [48], ShapeNet [9], and ABO [12]. We render the 3D objects through PyTorch3D [64] or Blender [13]. We utilize ControlNet [90] and Stable Diffusion [67] to simulate random visual variations. We primarily follow their default configurations. For the object appearance randomization in ObjectDR_{dis}, we set 10 steps in the DDIM sampler and inject an initial object guidance at step 3. Please refer to the supplementary material regarding color collection \mathcal{C}_c and material collection \mathcal{C}_m . For the background randomization, we set 20 steps in the DDIM sampler and construct scene collection \mathcal{C}_s using extensive scene categories [86, 93]. To filter synthesized images, we set $\tau = 0.95$.

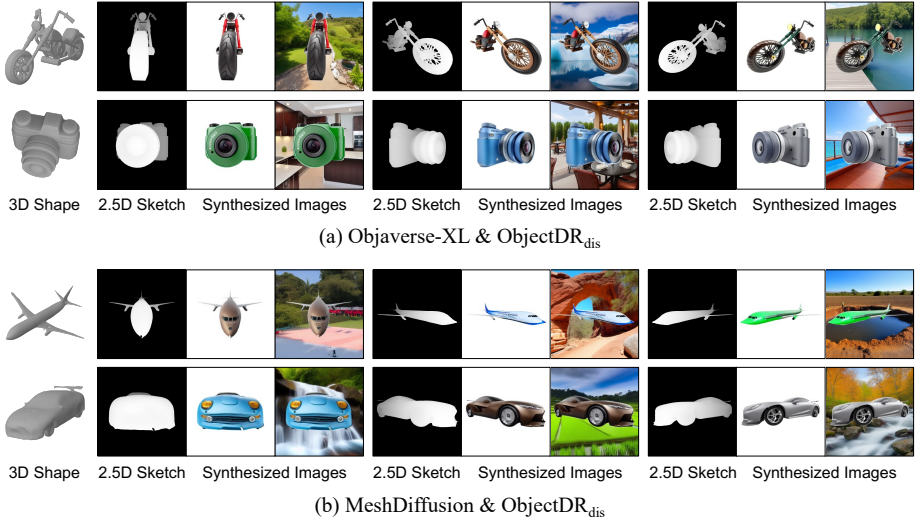


Fig. 4: Multi-view synthesis results of ObjectDR_{dis}. To obtain multi-view 2.5D sketches, we render 3D objects from Objaverse-XL [15] and MeshDiffusion [48] with multiple camera views. Using the 2.5D sketches as spatial conditions, we simulate diverse variations in object appearances and backgrounds via ControlNet [90]. In these visualization results, we show images generated during the object appearance randomization stage and the integration stage.

4.1 Analyses on Data Synthesis

Multi-view synthesis results. In the proposed framework, we render each 3D object with multiple camera views to obtain multi-view 2.5D sketches. As shown in Fig. 4, our framework simulates random visual variations in object appearances and backgrounds from each view. In this way, our synthesized images cover a wide range of distribution shifts. These randomized data could facilitate 3D shape reconstruction in the wild by encouraging a 3D shape estimation model to capture a domain-invariant geometry prior.

Comparison of image synthesis methods. In Fig. 5, we compare the original ObjectDR with ObjectDR_{dis}. When we utilize ObjectDR using “a [object]” as its textual condition, synthesized images mostly exhibit monotonous backgrounds due to the lack of background information (see Fig. 5(a)). To randomize object appearances and backgrounds, one could use “a [color] [material] [object] in the [scene]” as its textual condition. However, this approach compromises fidelity because the textual condition leads to the violation of spatial conditions (see Fig. 5(b)). Compared with them, ObjectDR_{dis} effectively preserves object silhouettes depicted in spatial conditions (see Fig. 5(c)) while integrating backgrounds via object silhouette masks (see Fig. 5(d)).

Effect of an initial guidance. Using the proposed disentangled framework, ObjectDR_{dis} substantially improves fidelity by leveraging an initial object guidance. Figure 6 shows that the initial guidance effectively forces the conditional diffusion model to precisely follow the given spatial condition. Note that the guidance provides a specific spatial structure, *i.e.*, an object silhouette and its white background. With the help of the object guidance, the diffusion model easily understands the contour of the object.



Fig. 5: Comparison of image synthesis methods. We render ShapeNet [9] objects to obtain 2.5D sketches. Then, we use the sketches as spatial conditions to synthesize images via ControlNet [90]. (a) ObjectDR using a textual condition “a [object]”. (b) ObjectDR using a textual condition “a [color] [material] [object] in the [scene]”. (c) ObjectDR_{dis} in the object appearance randomization stage. (d) ObjectDR_{dis} in the integration stage. We highlight regions with red circles.

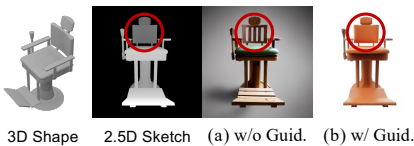


Fig. 6: Effect of an initial guidance. We use “a [color] [material] [object]” for the randomization. We highlight regions with red circles.



Fig. 7: Effect of different guidance injection steps out of 10 steps in the DDIM sampler. We magnify regions with red rectangles.

Different guidance injection steps. Figure 7 shows that feeding the guidance at step 1 leads to worse fidelity, since the guidance is more perturbed in order to be injected at step 1; it loses more spatial structure. When we inject the guidance at step 5, it leads to worse diversity; it preserves more specific details of the guidance (*e.g.*, gray texture).

Fidelity evaluation. From each synthetic dataset (see Fig. 8 & Sec. 4.2), we randomly sample 500 images and annotate their foreground object silhouette masks. Then, we compute IoU values between the annotated masks and the masks extracted from 2.5D sketches. Table 2 shows that ObjectDR_{dis} achieves an IoU value of 0.99, which is more than 10% higher compared with ObjectDR using a textual condition “a [color] [material] [object] in the [scene]”. Please refer to the supplementary material for details.

Diversity evaluation. We measure the diversity of each synthetic dataset in terms of the dissimilarity of images within a dataset (w/ LPIPS [91]) and the fraction of real data covered by synthetic data manifold (w/ improved recall [42]). For LPIPS, we compute the value for all possible pairs within a dataset and then average values. Table 2 shows that ObjectDR_{dis} images achieve the highest LPIPS; they are more perceptually diverse than other datasets. For the recall, we compute the value using Pix3D [75] as real data. As shown in Table 2, ObjectDR_{dis} images achieve the highest recall; our random simulation effectively covers real-world data. Please refer to the supplementary material for details.

Table 2: Evaluation of synthetic data regarding fidelity and diversity. Compared with computer graphics renderings, our data synthesis framework achieves higher diversity with similar fidelity without using texture and environment maps. Please refer to the supplementary material for details.

Data Synthesis	Asset Configuration			Fidelity	Diversity	
	3D Shape	Tex. Map	Env. Map	Mask IoU \uparrow	LPIPS \uparrow	Recall \uparrow
PyTorch3D [64]	ShapeNet [9]	Low-res.	–	1.000	0.390	0.021
ObjectDR	ShapeNet [9]	–	–	0.895	0.738	0.440
ObjectDR_{dis}	ShapeNet [9]	–	–	0.990	0.756	0.468
Blender [13]	ABO [12]	High-res.	HDRI	1.000	0.698	0.313
ObjectDR	ABO [12]	–	–	0.890	0.746	0.456
ObjectDR_{dis}	ABO [12]	–	–	0.991	0.753	0.474



Fig. 8: Comparison of computer graphics renderings. ShapeNet [9] objects are rendered through PyTorch3D [64], and ABO [12] objects are rendered through Blender [13]. To achieve high-quality results, high-resolution texture maps and HDRI maps are used for the rendering of ABO objects.

4.2 Data Synthesis for Model Pre-training

By pre-training a 3D shape estimation model on randomized data, the model is encouraged to generalize well across various environments. To validate the effectiveness of this pre-training, we synthesize a wide range of data via a random simulation. Specifically, we construct a large-scale dataset which consists of 110.8K ⟨3D shape, 2D image⟩-paired data using ShapeNet [9] shapes. In addition, we generate extra data using ABO [12] shapes for the comparison with high-quality computer graphics renderings produced by incorporating ABO shapes with high-resolution texture and HDRI maps.

3D object collections. ShapeNet [9] contains 55 object categories with 51.3K 3D object shapes and low-resolution texture maps, while ABO [12] contains 63 object categories with 8K 3D object shapes and high-resolution texture maps. Since ShapeNet contains a much larger number of 3D object shapes, we choose ShapeNet objects for the construction of our large-scale dataset. Among numerous object categories, we mainly utilize 3D object shapes from bed, chair, sofa and table categories in our experiments.

Data synthesis. For the data synthesis using ShapeNet [9] objects, we randomly select 200 bed objects and 2,500 objects from each category of chair, sofa and table. Also, we randomly select 30 objects from each of the other 51 categories. With the 9,230 ShapeNet objects, we synthesize 110.8K diverse images using Algorithm 1 with the setting of $K = 9230$, $N = 12$, and $M = 1$. For the data synthesis using ABO [12] objects, we utilize all the bed, chair, sofa and table objects to synthesize diverse images. Please refer to the supplementary material for more details.

Table 3: Evaluation of AtlasNet-Sphere [31] on Pix3D [75] \mathcal{S}_1 and \mathcal{S}_2 splits. We pre-train the model on synthetic data generated with ShapeNet [9] or ABO [12] objects, and then fine-tune it on the train set in each split. Please refer to the supplementary material for more results.

	Pre-training Data Synthesis	Asset Configuration			Chamfer Distance (10^{-3}) ↓				
		3D Shape	Tex. Map	Env. Map	bed	chair	sofa	table	mean
\mathcal{S}_1	–	–	–	–	7.4	15.7	5.3	29.1	14.4
	PyTorch3D [64]	ShapeNet [9]	Low-res.	–	7.1	14.8	5.2	28.2	13.8
	ObjectDR	ShapeNet [9]	–	–	6.9	14.4	5.2	26.8	13.3
	ObjectDR_{dis}	ShapeNet [9]	–	–	6.5	13.7	5.0	25.8	12.8
	Blender [13]	ABO [12]	High-res.	HDRI	7.0	14.5	5.2	27.2	13.5
	ObjectDR	ABO [12]	–	–	6.8	14.0	5.1	26.7	13.2
	ObjectDR_{dis}	ABO [12]	–	–	6.5	13.3	4.9	26.2	12.7
\mathcal{S}_2	–	–	–	–	28.9	18.5	5.7	59.5	28.2
	PyTorch3D [64]	ShapeNet [9]	Low-res.	–	27.9	17.5	5.9	55.9	26.8
	ObjectDR	ShapeNet [9]	–	–	26.2	17.0	5.7	52.3	25.3
	ObjectDR_{dis}	ShapeNet [9]	–	–	25.7	16.0	5.6	50.1	24.4
	Blender [13]	ABO [12]	High-res.	HDRI	27.4	17.1	5.8	52.8	25.8
	ObjectDR	ABO [12]	–	–	26.1	16.8	5.6	52.2	25.2
	ObjectDR_{dis}	ABO [12]	–	–	25.6	15.9	5.6	50.3	24.4

4.3 Evaluation with AtlasNet

In this subsection, we validate the effectiveness of the proposed model pre-training with AtlasNet-Sphere [31]. We pre-train the 3D shape reconstruction model for 20 epochs using synthetic data generated with ShapeNet [9] objects or ABO [12] objects. Then, we fine-tune the pre-trained model on Pix3D [9] if we do not specify otherwise. Please refer to the supplementary material for more details of the pre-training and fine-tuning.

Evaluation dataset and metric. The Pix3D [75] dataset contains 10K object images captured in real-world environments with 9 object categories including bed, chair, sofa and table. Following [28], we utilize train and test sets in two different splits (Pix3D \mathcal{S}_1 split & Pix3D \mathcal{S}_2 split) for comprehensive evaluation; 3D objects appeared in the train and test set are not disjoint in \mathcal{S}_1 split, whereas they are mutually exclusive in \mathcal{S}_2 split. Following [31, 58, 89], we align predicted and ground-truth meshes using ICP, and then compute the Chamfer distance with randomly sampled 10K points. Lower is better.

Effectiveness of the pre-training. Table 3 shows the evaluation results for the 4 object categories (bed, chair, sofa and table). In terms of the Chamfer distance, AtlasNet [31] achieves 0.0144 in \mathcal{S}_1 and 0.0282 in \mathcal{S}_2 without the model pre-training. When we pre-train the model on randomized data generated by ObjectDR_{dis}, the model accuracy is improved by 13.4% (0.0127 vs. 0.0144) in \mathcal{S}_1 and 15.6% (0.0244 vs. 0.0282) in \mathcal{S}_2 .

Comparison with the pre-training on computer graphics renderings. In Table 3, we compare ObjectDR_{dis} with PyTorch3D [64] and Blender [13]. When we pre-train AtlasNet [31] on PyTorch3D renderings, its accuracy is improved by 4.3% (0.0138 vs. 0.0144) in \mathcal{S}_1 and 5.2% (0.0268 vs. 0.0282) in \mathcal{S}_2 . When we pre-train the model on Blender renderings, its accuracy is improved by 6.7% (0.0135 vs. 0.0144) in \mathcal{S}_1 and 9.3% (0.0258 vs. 0.0282) in \mathcal{S}_2 . Compared with them, ObjectDR_{dis} shows better improvements (13.4% in \mathcal{S}_1 & 15.6% in \mathcal{S}_2) even without texture and environment maps.

Table 4: Evaluation of AtlasNet-Sphere [31] on Pix3D [75] \mathcal{S}_2 according to the model pre-training and fine-tuning. We pre-train the 3D shape reconstruction model on synthetic data generated with ShapeNet [9] objects, and then optionally fine-tune the model on the train set.

	Pre-training Data Synthesis	Pre-training	Fine-tuning	Chamfer Distance (10^{-3}) ↓				
				bed	chair	sofa	table	mean
\mathcal{S}_2	–	–	✓	28.9	18.5	5.7	59.5	28.2
	PyTorch3D [64]	✓	–	36.3	40.4	9.0	60.6	36.6
	ObjectDR	✓	–	28.5	23.9	7.8	54.8	28.8
	ObjectDR_{dis}	✓	–	26.7	22.0	7.7	52.1	27.1
	ObjectDR_{dis}	✓	✓	25.7	16.0	5.6	50.1	24.4

Table 5: Scale-up evaluation of pre-trained only AtlasNet-Sphere [31] on Pix3D [75] \mathcal{S}_2 . We generate data only using ABO [12] chair objects. Chamfer Distance (CD) is in 10^{-3} .

	Pre-training Data Synthesis	Data Scale	CD ↓
			chair
\mathcal{S}_2	Blender [13]	1×	18.3
	ObjectDR_{dis}	1×	17.0
	ObjectDR_{dis}	2×	14.8

Table 6: Ablation study on randomizing pre-training data. We pre-train AtlasNet-Sphere [31] on synthetic data generated with ShapeNet [9] objects, and then fine-tune the model on the train set in Pix3D [75] \mathcal{S}_2 . From untextured objects, we randomize their appearances and backgrounds.

	Pre-training Data	Chamfer Distance (10^{-3}) ↓				
		bed	chair	sofa	table	mean
\mathcal{S}_2	Plain Object Shapes	28.1	17.9	5.9	56.3	27.1
	+ Random Appearances	26.4	16.9	5.7	52.6	25.4
	+ Random Backgrounds	25.7	16.0	5.6	50.1	24.4

Comparison with the pre-training on ObjectDR images. In Table 3, we compare ObjectDR_{dis} with ObjectDR. When we pre-train AtlasNet [31] on ObjectDR images generated with a textual condition “a [color] [material] [object] in the [scene]”, its accuracy is improved by 9.1% (0.0132 vs. 0.0144) in \mathcal{S}_1 and 11.9% (0.0252 vs. 0.0282) in \mathcal{S}_2 . ObjectDR_{dis} shows better improvements (13.4% in \mathcal{S}_1 & 15.6% in \mathcal{S}_2), and it might be attributed to the superior fidelity and diversity shown in Table 2.

Pre-trained only model results. Table 4 shows the results from pre-trained models without the model fine-tuning on Pix3D [75]. When we pre-train AtlasNet [31] on our ObjectDR_{dis} images, it achieves 0.0271 in \mathcal{S}_2 . Compared with the model trained with Pix3D, the pre-trained only model shows better results (0.0271 vs. 0.0282) on Pix3D.

Scale-up evaluation. As described in Alg. 1, our framework generates M images per 2.5D sketch. By simply increasing the value of M , we could simulate more diverse object appearances and backgrounds. Note that computer graphics tools require more assets such as texture and environment maps for such diversification. In this scale-up evaluation, we pre-train AtlasNet [31] on ObjectDR_{dis} images generated only with ABO [12] chair objects using different M values. Table 5 shows pre-trained only model results on Pix3D [75] \mathcal{S}_2 . It achieves 0.0148 with $M = 2$, which is 23.6% better than the result with Blender [13] renderings and 14.9% better than the result with $M = 1$.

Ablation study on data synthesis. In Table 6, we evaluate the effect of random variations in object appearances and backgrounds. Compared with the pre-training on untextured object renderings, randomized object appearances improve its accuracy by 6.7%. Combining with random backgrounds, its accuracy is further improved by 4.1%.

Table 7: Evaluation of Mesh R-CNN [28] on Pix3D [75] \mathcal{S}_1 and \mathcal{S}_2 splits. We pre-train the 3D shape reconstruction model on synthetic data generated with ShapeNet [9] objects, and then fine-tune the pre-trained model on the train set in each split.

	Pre-training Data Synthesis	Average Precision (%) \uparrow									mean
		bed	bookcase	chair	desk	misc	sofa	table	tool	wardrobe	
\mathcal{S}_1	–	53.7	70.2	48.2	42.9	27.8	71.7	60.9	21.6	63.4	51.1
	PyTorch3D [64]	54.2	70.1	48.6	43.5	29.2	72.1	62.3	28.3	63.1	52.4
	ObjectDR	55.8	71.1	49.4	48.4	28.9	72.6	63.7	35.1	65.3	54.5
	ObjectDR_{dis}	57.3	70.8	51.2	48.2	30.5	73.8	67.1	39.2	67.2	56.2
\mathcal{S}_2	–	40.9	51.1	42.7	18.2	0.0	70.8	27.2	5.2	2.9	28.8
	PyTorch3D [64]	41.6	51.2	44.3	19.8	0.0	71.6	28.3	8.3	2.8	29.8
	ObjectDR	43.1	53.6	45.0	25.9	0.0	72.5	28.7	9.1	4.4	31.4
	ObjectDR_{dis}	44.9	53.1	48.1	27.4	0.0	73.6	31.8	12.9	5.8	33.1



Fig. 9: Estimation results of Mesh R-CNN [28] on Pix3D \mathcal{S}_1 [75]. Compared with the model without the pre-training, the model pre-trained on ObjectDR_{dis} images estimates more precise object shapes appeared in real-world environments. We highlight regions with red circles.

4.4 Evaluation with Mesh R-CNN

In this subsection, we validate the effectiveness of the proposed model pre-training with Mesh R-CNN [28]. We pre-train the 3D shape reconstruction model for 20 epochs using synthetic data generated with ShapeNet [9] objects. Then, we fine-tune the pre-trained model on Pix3D [9] if we do not specify otherwise. Please refer to the supplementary material for more details of the pre-training and fine-tuning.

Evaluation dataset and metric. For this evaluation, we also use Pix3D [75] \mathcal{S}_1 and \mathcal{S}_2 splits introduced by Mesh R-CNN [28]. Following Mesh R-CNN, we randomly sample 10K points uniformly from the surfaces of both predicted and ground-truth meshes, and then compute the average precision (higher is better) considering $F1^{0.3} > 0.5$ as a true-positive; $F1^{0.3}$ is the harmonic mean of precision and recall, representing the concordance between predicted and ground-truth points within a distance threshold 0.3. Please refer to the supplementary material for more details of the evaluation metric.

Effectiveness of the pre-training. Table 7 shows the evaluation results for all the 9 object categories in Pix3D [75]. In terms of the average precision, Mesh R-CNN [28] achieves 51.1 in \mathcal{S}_1 and 28.8 in \mathcal{S}_2 without the model pre-training. When we pre-train the model on randomized data generated by ObjectDR_{dis}, the model accuracy is improved by 10.0% (56.2 vs. 51.1) in \mathcal{S}_1 and 14.9% (33.1 vs. 28.8) in \mathcal{S}_2 . To qualitatively evaluate the effect of the model pre-training, we compare model estimation results in Fig. 9. The results demonstrate that the proposed pre-training helps the model to precisely estimate object shapes appeared in real-world environments.



Fig. 10: Estimation results of pre-trained only Mesh R-CNN [28] for *unseen synthetic images* generated by ObjectDR or ObjectDR_{dis}. ObjectDR sometimes distorts the object shape depicted in the spatial condition, which leads to less stable pre-training. We highlight regions with red circles.

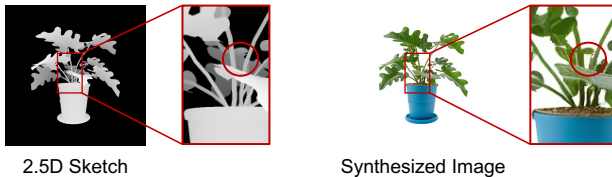


Fig. 11: Imperfect synthesis result. Although ObjectDR_{dis} substantially improves fidelity, results are not always flawless. We magnify and highlight regions with red rectangles and circles.

Comparison with the pre-training on ObjectDR images. We compare ObjectDR_{dis} with ObjectDR in Table 7. When we pre-train Mesh R-CNN [28] on ObjectDR images generated with a textual condition “a [color] [material] [object] in the [scene]”, its accuracy is improved by 6.7% (54.5 vs. 51.1) in S_1 and 9.0% (31.4 vs. 28.8) in S_2 . To analyze why ObjectDR_{dis} achieves superior improvements (10.0% in S_1 & 14.9% in S_2), we also compare their estimation results in Fig. 10. It shows that the model pre-trained on ObjectDR images produces more noisy outputs. This might be attributed to unstable pre-training caused by distorted shapes in ObjectDR images (see Fig. 5 & Table 2).

5 Limitation

As shown in Table 2, ObjectDR_{dis} produces high-fidelity synthetic data. However, minor disparities might still be observable as shown in Fig. 11. For this reason, we utilize synthesized images only for the model pre-training. Note that this issue would be alleviated with the development of conditional generative models.

6 Conclusion

We have presented a scalable \langle 3D shape, 2D image \rangle -paired data synthesis framework using a random simulation. To effectively tackle the trade-off between diversity and fidelity, we introduced a disentangled framework. We validated that our randomized data substantially improved 3D shape reconstruction models on a real-world benchmark.

Acknowledgments. This work was supported by ADD grant funded by the Korean government. T.-H. Oh and K. Youwang were partially supported by IITP grant funded by the Korean government (MSIT) (No.2020-0-00004 (10%), Development of Previsional Intelligence based on Long-term Visual Memory Network; No.2021-0-02068 (10%), Artificial Intelligence Innovation Hub)

References

1. Alwala, K.V., Gupta, A., Tulsiani, S.: Pre-train, Self-train, Distill: A simple recipe for Super-sizing 3D Reconstruction. In: Proceedings of the IEEE/CVF Conference on Computer Vision and Pattern Recognition (CVPR) (2022) [3](#), [4](#)
2. Aubry, M., Maturana, D., Efros, A.A., Russell, B.C., Sivic, J.: Seeing 3D Chairs: Exemplar Part-based 2D-3D Alignment using a Large Dataset of CAD Models. In: Proceedings of the IEEE Conference on Computer Vision and Pattern Recognition (CVPR) (2014) [4](#)
3. Bae, G., de La Gorce, M., Baltrusaitis, T., Hewitt, C., Chen, D., Valentin, J., Cipolla, R., Shen, J.: DigiFace-1M: 1 Million Digital Face Images for Face Recognition. In: IEEE/CVF Winter Conference on Applications of Computer Vision (WACV) (2023) [4](#)
4. Beery, S., Liu, Y., Morris, D., Piavis, J., Kapoor, A., Meister, M., Joshi, N., Perona, P.: Synthetic Examples Improve Generalization for Rare Classes. In: IEEE/CVF Winter Conference on Applications of Computer Vision (WACV) (2020) [4](#)
5. Black, M.J., Patel, P., Tesch, J., Yang, J.: BEDLAM: A Synthetic Dataset of Bodies Exhibiting Detailed Lifelike Animated Motion. In: Proceedings of the IEEE/CVF Conference on Computer Vision and Pattern Recognition (CVPR) (2023) [4](#)
6. Carlini, N., Tramer, F., Wallace, E., Jagielski, M., Herbert-Voss, A., Lee, K., Roberts, A., Brown, T., Song, D., Erlingsson, U., Oprea, A., Raffel, C.: Extracting Training Data from Large Language Models. In: 30th USENIX Security Symposium (USENIX Security 21) (2021) [26](#)
7. Carlucci, F.M., D’Innocente, A., Bucci, S., Caputo, B., Tommasi, T.: Domain Generalization by Solving Jigsaw Puzzles. In: Proceedings of the IEEE/CVF Conference on Computer Vision and Pattern Recognition (CVPR) (2019) [4](#)
8. Caron, M., Touvron, H., Misra, I., Jégou, H., Mairal, J., Bojanowski, P., Joulin, A.: Emerging Properties in Self-Supervised Vision Transformers. In: Proceedings of the IEEE/CVF International Conference on Computer Vision (ICCV) (2021) [1](#)
9. Chang, A.X., Funkhouser, T., Guibas, L., Hanrahan, P., Huang, Q., Li, Z., Savarese, S., Savva, M., Song, S., Su, H., Xiao, J., Yi, L., Yu, F.: ShapeNet: An Information-Rich 3D Model Repository. arXiv preprint arXiv:1512.03012 (2015) [1](#), [3](#), [4](#), [5](#), [7](#), [9](#), [10](#), [11](#), [12](#), [13](#), [21](#), [23](#), [24](#), [25](#)
10. Chou, G., Bahat, Y., Heide, F.: Diffusion-SDF: Conditional Generative Modeling of Signed Distance Functions. In: Proceedings of the IEEE/CVF International Conference on Computer Vision (ICCV) (2023) [3](#)
11. Choy, C.B., Xu, D., Gwak, J., Chen, K., Savarese, S.: 3D-R2N2: A Unified Approach for Single and Multi-view 3D Object Reconstruction. In: Proceedings of the European Conference on Computer Vision (ECCV) (2016) [3](#)
12. Collins, J., Goel, S., Deng, K., Luthra, A., Xu, L., Gundogdu, E., Zhang, X., Vicente, T.F.Y., Dideriksen, T., Arora, H., Guillaumin, M., Malik, J.: ABO: Dataset and Benchmarks for Real-World 3D Object Understanding. In: Proceedings of the IEEE/CVF Conference on Computer Vision and Pattern Recognition (CVPR) (2022) [1](#), [3](#), [4](#), [5](#), [7](#), [10](#), [11](#), [12](#), [23](#), [25](#)
13. Community, B.O.: Blender - a 3D modelling and rendering package. Blender Foundation (2018) [7](#), [10](#), [11](#), [12](#), [25](#)
14. Dehban, A., Borrego, J., Figueiredo, R., Moreno, P., Bernardino, A., Santos-Victor, J.: The impact of domain randomization on object detection: A case study on parametric shapes and synthetic textures. In: IEEE/RSJ International Conference on Intelligent Robots and Systems (IROS) (2019) [4](#)
15. Deitke, M., Liu, R., Wallingford, M., Ngo, H., Michel, O., Kusupati, A., Fan, A., Laforte, C., Voleti, V., Gadre, S.Y., VanderBilt, E., Kembhavi, A., Vondrick, C., Gkioxari, G., Ehsani, K., Schmidt, L., Farhadi, A.: Objaverse-XL: A Universe of 10M+ 3D Objects. In: Advances in Neural Information Processing Systems (NeurIPS) (2023) [1](#), [3](#), [4](#), [5](#), [7](#), [8](#)

16. Deitke, M., Schwenk, D., Salvador, J., Weihs, L., Michel, O., Vanderbilt, E., Schmidt, L., Ehsani, K., Kembhavi, A., Farhadi, A.: Objaverse: A Universe of Annotated 3D Objects. In: Proceedings of the IEEE/CVF Conference on Computer Vision and Pattern Recognition (CVPR) (2023) [3](#)
17. Delanoy, J., Aubry, M., Isola, P., Efros, A.A., Bousseau, A.: 3D Sketching using Multi-View Deep Volumetric Prediction. In: ACM on Computer Graphics and Interactive Techniques (2018) [4](#)
18. Dosovitskiy, A., Fischer, P., Ilg, E., Hausser, P., Hazirbas, C., Golkov, V., Van Der Smagt, P., Cremers, D., Brox, T.: FlowNet: Learning optical flow with convolutional networks. In: Proceedings of the IEEE International Conference on Computer Vision (ICCV) (2015) [4](#)
19. Dou, Q., Castro, D.C., Kamnitsas, K., Glocker, B.: Domain Generalization via Model-Agnostic Learning of Semantic Features. In: Advances in Neural Information Processing Systems (NeurIPS) (2019) [4](#)
20. Esser, P., Rombach, R., Ommer, B.: A Note on Data Biases in Generative Models. In: NeurIPS 2020 Workshop on Machine Learning for Creativity and Design (2020) [26](#)
21. Exarchos, I., Jiang, Y., Yu, W., Liu, C.K.: Policy Transfer via Kinematic Domain Randomization and Adaptation. In: International Conference on Robotics and Automation (ICRA) (2021) [4](#)
22. Fu, H., Cai, B., Gao, L., Zhang, L., Li, J.W.C., Xun, Z., Sun, C., Jia, R., Zhao, B., Zhang, H.: 3D-FRONT: 3D Furnished Rooms with layOuts and semaNTics. In: Proceedings of the IEEE/CVF International Conference on Computer Vision (ICCV) (2021) [4](#)
23. Gaidon, A., Wang, Q., Cabon, Y., Vig, E.: Virtual worlds as proxy for multi-object tracking analysis. In: Proceedings of the IEEE Conference on Computer Vision and Pattern Recognition (CVPR). pp. 4340–4349 (2016) [4](#)
24. Gandikota, R., Materzynska, J., Fiotto-Kaufman, J., Bau, D.: Erasing Concepts from Diffusion Models. In: Proceedings of the IEEE/CVF International Conference on Computer Vision (ICCV) (2023) [26](#)
25. Genova, K., Cole, F., Sud, A., Sarna, A., Funkhouser, T.: Local Deep Implicit Functions for 3D Shape. In: Proceedings of the IEEE/CVF Conference on Computer Vision and Pattern Recognition (CVPR) (2020) [3](#)
26. Ghiasi, G., Cui, Y., Srinivas, A., Qian, R., Lin, T.Y., Cubuk, E.D., Le, Q.V., Zoph, B.: Simple copy-paste is a strong data augmentation method for instance segmentation. In: Proceedings of the IEEE/CVF Conference on Computer Vision and Pattern Recognition (CVPR) (2021) [4](#)
27. Girdhar, R., Fouhey, D.F., Rodriguez, M., Gupta, A.: Learning a Predictable and Generative Vector Representation for Objects. In: Proceedings of the European Conference on Computer Vision (ECCV) (2016) [3](#)
28. Gkioxari, G., Malik, J., Johnson, J.: Mesh R-CNN. In: Proceedings of the IEEE/CVF International Conference on Computer Vision (ICCV) (2019) [3](#), [7](#), [11](#), [13](#), [14](#), [22](#), [26](#)
29. Goel, S., Kanazawa, A., Malik, J.: Shape and Viewpoint without Keypoints. In: Proceedings of the European Conference on Computer Vision (ECCV) (2020) [3](#)
30. Greff, K., Belletti, F., Beyer, L., Doersch, C., Du, Y., Duckworth, D., Fleet, D.J., Gnanaprasam, D., Golemo, F., Herrmann, C., Kipf, T., Kundu, A., Lagun, D., Laradji, I., Hsueh-Ti, Liu, Meyer, H., Miao, Y., Nowrouzezahrai, D., Oztireli, C., Pot, E., Radwan, N., Rebain, D., Sabour, S., Sajjadi, M.S.M., Sela, M., Sitzmann, V., Stone, A., Sun, D., Vora, S., Wang, Z., Wu, T., Yi, K.M., Zhong, F., Tagliasacchi, A.: Kubric: A Scalable Dataset Generator. In: Proceedings of the IEEE/CVF Conference on Computer Vision and Pattern Recognition (CVPR) (2022) [4](#)
31. Groueix, T., Fisher, M., Kim, V.G., Russell, B.C., Aubry, M.: AtlasNet: A Papier-Mâché Approach to Learning 3D Surface Generation. In: Proceedings of the IEEE Conference on Computer Vision and Pattern Recognition (CVPR) (2018) [3](#), [7](#), [11](#), [12](#), [22](#), [23](#), [25](#)

32. Hoffmann, D.T., Tzionas, D., Black, M.J., Tang, S.: Learning to train with synthetic humans. In: DAGM German Conference on Pattern Recognition (GCPR). Springer (2019) 4
33. Huang, J., Guan, D., Xiao, A., Lu, S.: FSDR: Frequency Space Domain Randomization for Domain Generalization. In: Proceedings of the IEEE/CVF Conference on Computer Vision and Pattern Recognition (CVPR) (2021) 4
34. Kanazawa, A., Tulsiani, S., Efros, A.A., Malik, J.: Learning Category-Specific Mesh Reconstruction from Image Collections. In: Proceedings of the European Conference on Computer Vision (ECCV) (2018) 3
35. Kang, M., Zhu, J.Y., Zhang, R., Park, J., Shechtman, E., Paris, S., Park, T.: Scaling up GANs for Text-to-Image Synthesis. In: Proceedings of the IEEE/CVF Conference on Computer Vision and Pattern Recognition (CVPR) (2023) 1
36. Kar, A., Prakash, A., Liu, M.Y., Cameracci, E., Yuan, J., Rusiniak, M., Acuna, D., Torralba, A., Fidler, S.: Meta-Sim: Learning to Generate Synthetic Datasets. In: Proceedings of the IEEE/CVF International Conference on Computer Vision (ICCV) (2019) 4
37. Kim, D., Saito, K., Oh, T.H., Plummer, B.A., Sclaroff, S., Saenko, K.: Cross-domain Self-supervised Learning for Domain Adaptation with Few Source Labels. In: Proceedings of the IEEE/CVF International Conference on Computer Vision (ICCV) (2021) 4
38. Kingma, D.P., Ba, J.: Adam: A Method for Stochastic Optimization. In: International Conference on Learning Representations (ICLR) (2015) 22
39. Kirillov, A., Mintun, E., Ravi, N., Mao, H., Rolland, C., Gustafson, L., Xiao, T., Whitehead, S., Berg, A.C., Lo, W.Y., Dollár, P., Girshick, R.: Segment Anything. In: Proceedings of the IEEE/CVF International Conference on Computer Vision (ICCV) (2023) 1
40. Koch, S., Matveev, A., Jiang, Z., Williams, F., Artemov, A., Burnaev, E., Alexa, M., Zorin, D., Panozzo, D.: ABC: A Big CAD Model Dataset For Geometric Deep Learning. In: Proceedings of the IEEE/CVF Conference on Computer Vision and Pattern Recognition (CVPR) (2019) 3
41. Koh, P.W., Sagawa, S., Marklund, H., Xie, S.M., Zhang, M., Balsubramani, A., Hu, W., Yasunaga, M., Phillips, R.L., Gao, I., Lee, T., David, E., Stavness, I., Guo, W., Earnshaw, B.A., Haque, I.S., Beery, S., Leskovec, J., Kundaje, A., Pierson, E., Levine, S., Finn, C., Liang, P.: WILDS: A Benchmark of in-the-Wild Distribution Shifts. In: International Conference on Machine Learning (ICML) (2021) 4
42. Kynkäänniemi, T., Karras, T., Laine, S., Lehtinen, J., Aila, T.: Improved Precision and Recall Metric for Assessing Generative Models. In: Advances in Neural Information Processing Systems (NeurIPS) (2019) 9, 22
43. Li, D., Zhang, J., Yang, Y., Liu, C., Song, Y.Z., Hospedales, T.M.: Episodic Training for Domain Generalization. In: Proceedings of the IEEE/CVF International Conference on Computer Vision (ICCV) (2019) 4
44. Li, F., Zhang, H., Sun, P., Zou, X., Liu, S., Yang, J., Li, C., Zhang, L., Gao, J.: Semantic-SAM: Segment and Recognize Anything at Any Granularity. arXiv preprint arXiv:2307.04767 (2023) 1
45. Li, Y., Liu, H., Wu, Q., Mu, F., Yang, J., Gao, J., Li, C., Lee, Y.J.: GLIGEN: Open-Set Grounded Text-to-Image Generation. In: Proceedings of the IEEE/CVF Conference on Computer Vision and Pattern Recognition (CVPR) (2023) 1, 2, 3, 4, 23
46. Liu, H., Zheng, Y., Chen, G., Cui, S., Han, X.: Towards High-Fidelity Single-view Holistic Reconstruction of Indoor Scenes. In: Proceedings of the European Conference on Computer Vision (ECCV) (2022) 3
47. Liu, R., Wu, R., Hoorick, B.V., Tokmakov, P., Zakharov, S., Vondrick, C.: Zero-1-to-3: Zero-shot One Image to 3D Object. In: Proceedings of the IEEE/CVF International Conference on Computer Vision (ICCV) (2023) 1, 26
48. Liu, Z., Feng, Y., Black, M.J., Nowrouzezahrai, D., Paull, L., Liu, W.: MeshDiffusion: Score-based Generative 3D Mesh Modeling. In: International Conference on Learning Representations (ICLR) (2023) 1, 3, 5, 7, 8

49. Long, X., Guo, Y.C., Lin, C., Liu, Y., Dou, Z., Liu, L., Ma, Y., Zhang, S.H., Habermann, M., Theobalt, C., Wang, W.: Wonder3D: Single Image to 3D using Cross-Domain Diffusion. In: Proceedings of the IEEE/CVF Conference on Computer Vision and Pattern Recognition (CVPR) (2024) [26](#)
50. Mahajan, D., Tople, S., Sharma, A.: Domain Generalization using Causal Matching. In: International Conference on Machine Learning (ICML) (2021) [4](#)
51. Matsuura, T., Harada, T.: Domain Generalization Using a Mixture of Multiple Latent Domains. In: Proceedings of the AAAI Conference on Artificial Intelligence (AAAI) (2020) [4](#)
52. Mayer, N., Ilg, E., Hausser, P., Fischer, P., Cremers, D., Dosovitskiy, A., Brox, T.: A large dataset to train convolutional networks for disparity, optical flow, and scene flow estimation. In: Proceedings of the IEEE Conference on Computer Vision and Pattern Recognition (CVPR) (2016) [4](#)
53. Mehta, B., Diaz, M., Golemo, F., Pal, C.J., Paull, L.: Active Domain Randomization. In: Conference on Robot Learning (CoRL) (2019) [4](#)
54. Meng, C., He, Y., Song, Y., Song, J., Wu, J., Zhu, J.Y., Ermon, S.: SDEdit: Guided Image Synthesis and Editing with Stochastic Differential Equations. In: International Conference on Learning Representations (ICLR) (2022) [7](#)
55. Mescheder, L., Oechsle, M., Niemeyer, M., Nowozin, S., Geiger, A.: Occupancy Networks: Learning 3D Reconstruction in Function Space. In: Proceedings of the IEEE/CVF Conference on Computer Vision and Pattern Recognition (CVPR) (2019) [3](#)
56. Mou, C., Wang, X., Xie, L., Wu, Y., Zhang, J., Qi, Z., Shan, Y., Qie, X.: T2I-Adapter: Learning Adapters to Dig out More Controllable Ability for Text-to-Image Diffusion Models. arXiv preprint arXiv:2302.08453 (2023) [1](#), [2](#), [3](#), [4](#), [23](#)
57. Ni, Z., Wei, L., Li, J., Tang, S., Zhuang, Y., Tian, Q.: Degeneration-Tuning: Using Scrambled Grid shield Unwanted Concepts from Stable Diffusion. In: 31st ACM International Conference on Multimedia (2023) [26](#)
58. Nie, Y., Han, X., Guo, S., Zheng, Y., Chang, J., Zhang, J.J.: Total3DUnderstanding: Joint Layout, Object Pose and Mesh Reconstruction for Indoor Scenes from a Single Image. In: Proceedings of the IEEE/CVF Conference on Computer Vision and Pattern Recognition (CVPR) (2020) [3](#), [11](#), [22](#)
59. Pan, J., Han, X., Chen, W., Tang, J., Jia, K.: Deep Mesh Reconstruction from Single RGB Images via Topology Modification Networks. In: Proceedings of the IEEE/CVF International Conference on Computer Vision (ICCV) (2019) [3](#)
60. Prakash, A., Boochoon, S., Brophy, M., Acuna, D., Cameracci, E., State, G., Shapira, O., Birchfield, S.: Structured Domain Randomization: Bridging the Reality Gap by Context-Aware Synthetic Data. In: International Conference on Robotics and Automation (ICRA) (2019) [4](#)
61. Qin, C., Zhang, S., Yu, N., Feng, Y., Yang, X., Zhou, Y., Wang, H., Niebles, J.C., Xiong, C., Savarese, S., Ermon, S., Fu, Y., Xu, R.: UniControl: A Unified Diffusion Model for Controllable Visual Generation In the Wild. In: Advances in Neural Information Processing Systems (NeurIPS) (2023) [1](#), [2](#), [3](#), [4](#), [23](#)
62. Radford, A., Kim, J.W., Hallacy, C., Ramesh, A., Goh, G., Agarwal, S., Sastry, G., Askell, A., Mishkin, P., Clark, J., Krueger, G., Sutskever, I.: Learning Transferable Visual Models From Natural Language Supervision. In: International Conference on Machine Learning (ICML) (2021) [1](#)
63. Ranjan, A., Hoffmann, D.T., Tzionas, D., Tang, S., Romero, J., Black, M.J.: Learning multi-human optical flow. International Journal of Computer Vision (IJCV) **128**, 873–890 (2020) [4](#)
64. Ravi, N., Reizenstein, J., Novotny, D., Gordon, T., Lo, W.Y., Johnson, J., Gkioxari, G.: Accelerating 3D Deep Learning with PyTorch3D. arXiv preprint arXiv:2007.08501 (2020) [7](#), [10](#), [11](#), [12](#), [13](#), [21](#), [25](#)

65. Ren, X., Luo, J., Solowjow, E., Ojea, J.A., Gupta, A., Tamar, A., Abbeel, P.: Domain Randomization for Active Pose Estimation. In: International Conference on Robotics and Automation (ICRA) (2019) [4](#)
66. Richter, S.R., Vineet, V., Roth, S., Koltun, V.: Playing for data: Ground truth from computer games. In: Proceedings of the European Conference on Computer Vision (ECCV). Springer (2016) [4](#)
67. Rombach, R., Blattmann, A., Lorenz, D., Esser, P., Ommer, B.: High-Resolution Image Synthesis with Latent Diffusion Models. In: Proceedings of the IEEE/CVF Conference on Computer Vision and Pattern Recognition (CVPR) (2022) [1](#), [4](#), [7](#)
68. Russakovsky, O., Deng, J., Su, H., Krause, J., Satheesh, S., Ma, S., Huang, Z., Karpathy, A., Khosla, A., Bernstein, M., Berg, A.C., Fei-Fei, L.: ImageNet Large Scale Visual Recognition Challenge. In: International Journal of Computer Vision (IJCV) (2015) [1](#)
69. Schuhmann, C., Beaumont, R., Vencu, R., Gordon, C., Wightman, R., Cherti, M., Coombes, T., Katta, A., Mullis, C., Wortsman, M., Schramowski, P., Kundurthy, S., Crowson, K., Schmidt, L., Kaczmarczyk, R., Jitsev, J.: LAION-5B: An open large-scale dataset for training next generation image-text models. In: Advances in Neural Information Processing Systems (NeurIPS) (2022) [1](#)
70. Schuhmann, C., Vencu, R., Beaumont, R., Kaczmarczyk, R., Mullis, C., Katta, A., Coombes, T., Jitsev, J., Komatsuzaki, A.: LAION-400M: Open Dataset of CLIP-Filtered 400 Million Image-Text Pairs. arXiv preprint arXiv:2111.02114 (2021) [1](#)
71. Seo, S., Suh, Y., Kim, D., Kim, G., Han, J., Han, B.: Learning to Optimize Domain Specific Normalization for Domain Generalization. In: Proceedings of the European Conference on Computer Vision (ECCV) (2020) [4](#)
72. Shim, J., Kang, C., Joo, K.: Diffusion-Based Signed Distance Fields for 3D Shape Generation. In: Proceedings of the IEEE/CVF Conference on Computer Vision and Pattern Recognition (CVPR) (2023) [3](#)
73. Simonyan, Karen and Zisserman, Andrew: Very deep convolutional networks for large-scale image recognition. In: International Conference on Learning Representations (ICLR) (2015) [22](#)
74. Sun, D., Vlasic, D., Herrmann, C., Jampani, V., Krainin, M., Chang, H., Zabih, R., Freeman, W.T., Liu, C.: Autoflow: Learning a better training set for optical flow. In: Proceedings of the IEEE/CVF Conference on Computer Vision and Pattern Recognition (CVPR) (2021) [4](#)
75. Sun, X., Wu, J., Zhang, X., Zhang, Z., Zhang, C., Xue, T., Tenenbaum, J.B., Freeman, W.T.: Pix3D: Dataset and Methods for Single-Image 3D Shape Modeling. In: Proceedings of the IEEE/CVF Conference on Computer Vision and Pattern Recognition (CVPR) (2018) [3](#), [9](#), [11](#), [12](#), [13](#), [22](#), [23](#), [25](#)
76. Tobin, J., Fong, R., Ray, A., Schneider, J., Zaremba, W., Abbeel, P.: Domain Randomization for Transferring Deep Neural Networks from Simulation to the Real World. In: IEEE/RSJ International Conference on Intelligent Robots and Systems (IROS) (2017) [4](#)
77. Tremblay, J., Prakash, A., Acuna, D., Brophy, M., Jampani, V., Anil, C., To, T., Cameracci, E., Bochoon, S., Birchfield, S.: Training Deep Networks With Synthetic Data: Bridging the Reality Gap by Domain Randomization. In: IEEE Conference on Computer Vision and Pattern Recognition (CVPR) Workshops (2018) [4](#)
78. Tulsiani, S., Zhou, T., Efros, A.A., Malik, J.: Multi-view supervision for single-view reconstruction via differentiable ray consistency. In: Proceedings of the IEEE Conference on Computer Vision and Pattern Recognition (CVPR) (2017) [3](#), [4](#)
79. de Vries, T., Misra, I., Wang, C., van der Maaten, L.: Does Object Recognition Work for Everyone? In: Proceedings of the IEEE/CVF Conference on Computer Vision and Pattern Recognition (CVPR) Workshops (2019) [26](#)

80. Wang, N., Zhang, Y., Li, Z., Fu, Y., Liu, W., Jiang, Y.G.: Pixel2Mesh: Generating 3D Mesh Models from Single RGB Images. In: Proceedings of the European Conference on Computer Vision (ECCV) (2018) [3](#)
81. Wang, Z., Wang, Y., Chen, Y., Xiang, C., Chen, S., Yu, D., Li, C., Su, H., Zhu, J.: CRM: Single Image to 3D Textured Mesh with Convolutional Reconstruction Model. arXiv preprint arXiv:2403.05034 (2024) [26](#)
82. Wood, E., Baltrušaitis, T., Hewitt, C., Dziadzio, S., Johnson, M., Estellers, V., Cashman, T.J., Shotton, J.: Fake It Till You Make It: Face analysis in the wild using synthetic data alone. In: Proceedings of the IEEE/CVF International Conference on Computer Vision (ICCV) (2021) [4](#)
83. Wu, J., Wang, Y., Xue, T., Sun, X., Freeman, W.T., Tenenbaum, J.B.: MarrNet: 3D Shape Reconstruction via 2.5D Sketches. In: Advances in Neural Information Processing Systems (NIPS) (2017) [3](#)
84. Wu, J., Zhang, C., Xue, T., Freeman, W.T., Tenenbaum, J.B.: Learning a Probabilistic Latent Space of Object Shapes via 3D Generative-Adversarial Modeling. In: Advances in Neural Information Processing Systems (NIPS) (2017) [3](#)
85. Wu, J., Zhang, C., Zhang, X., Zhang, Z., Freeman, W.T., Tenenbaum, J.B.: Learning Shape Priors for Single-View 3D Completion and Reconstruction. In: Proceedings of the European Conference on Computer Vision (ECCV) (2018) [3](#)
86. Xiao, J., Hays, J., Ehinger, K.A., Oliva, A., Torralba, A.: SUN database: Large-scale scene recognition from abbey to zoo. In: Proceedings of the IEEE Conference on Computer Vision and Pattern Recognition (CVPR) (2010) [7](#)
87. Yeh, Y.Y., Nagano, K., Khamis, S., Kautz, J., Liu, M.Y., Wang, T.C.: Learning to Relight Portrait Images via a Virtual Light Stage and Synthetic-to-Real Adaptation. ACM Transactions on Graphics (Proc. SIGGRAPH Asia) (2022) [4](#)
88. Yue, X., Zhang, Y., Zhao, S., Sangiovanni-Vincentelli, A., Keutzer, K., Gong, B.: Domain Randomization and Pyramid Consistency: Simulation-to-Real Generalization Without Accessing Target Domain Data. In: Proceedings of the IEEE/CVF International Conference on Computer Vision (ICCV) (2019) [4](#)
89. Zhang, C., Cui, Z., Zhang, Y., Zeng, B., Pollefeys, M., Liu, S.: Holistic 3D Scene Understanding from a Single Image with Implicit Representation. In: Proceedings of the IEEE/CVF Conference on Computer Vision and Pattern Recognition (CVPR) (2021) [3](#), [11](#), [22](#)
90. Zhang, L., Rao, A., Agrawala, M.: Adding Conditional Control to Text-to-Image Diffusion Models. In: Proceedings of the IEEE/CVF International Conference on Computer Vision (ICCV) (2023) [1](#), [2](#), [3](#), [4](#), [6](#), [7](#), [8](#), [9](#), [23](#), [25](#)
91. Zhang, R., Isola, P., Efros, A.A., Shechtman, E., Wang, O.: The Unreasonable Effectiveness of Deep Features as a Perceptual Metric. In: Proceedings of the IEEE/CVF Conference on Computer Vision and Pattern Recognition (CVPR) (2018) [9](#), [22](#)
92. Zhang, X., Zhang, Z., Zhang, C., Tenenbaum, J.B., Freeman, W.T., Wu, J.: Learning to Reconstruct Shapes from Unseen Classes. In: Advances in Neural Information Processing Systems (NeurIPS) (2018) [3](#)
93. Zhou, B., Lapedriza, A., Khosla, A., Oliva, A., Torralba, A.: Places: A 10 Million Image Database for Scene Recognition. In: IEEE Transactions on Pattern Analysis and Machine Intelligence (TPAMI) (2018) [7](#)
94. Zhou, K., Yang, Y., Hospedales, T., Xiang, T.: Learning to Generate Novel Domains for Domain Generalization. In: Proceedings of the European Conference on Computer Vision (ECCV) (2020) [4](#)
95. Zhou, K., Yang, Y., Qiao, Y., Xiang, T.: Domain Generalization with MixStyle. In: International Conference on Learning Representations (ICLR) (2021) [4](#)

Object-Centric Domain Randomization for 3D Shape Reconstruction in the Wild

— Supplementary Material —

Junhyeong Cho¹ Kim Youwang² Hunmin Yang^{1,4} Tae-Hyun Oh^{2,3,5}

¹ADD ²Department of EE, POSTECH ³Graduate School of AI, POSTECH ⁴KAIST

⁵Institute for Convergence Research and Education in Advanced Technology, Yonsei University

<https://ObjectDR.github.io>

This supplementary material provides additional implementation details (Sec. **A**), training details (Sec. **B**), evaluation details (Sec. **C**), experimental results (Sec. **D**), discussion (Sec. **E**) and ethics considerations (Sec. **F**), which are not included in the main paper due to its limited space.

A Additional Implementation Details

Object rendering with multiple camera views. To construct our large-scale dataset, we render each ShapeNet [9] object with $N = 12$ camera views using the renderer in PyTorch3D [64]. Specifically, we randomly set azimuth angles within the range of -180° to 180° and elevation angles within the range of -20° to 20° . From each view, the renderer produces a 512×512 resolution image and its corresponding 2.5D sketch.

Color and material collections. We randomize visual variations in object appearances using a textual condition “a [color] [material] [object]”, where [color] and [material] are randomly selected from color collection \mathcal{C}_c and material collection \mathcal{C}_m , respectively. For the color collection \mathcal{C}_c , we include “red”, “pink”, “orange”, “yellow”, “green”, “blue”, “purple”, “brown”, “white”, “black” and “gray”. For the material collection \mathcal{C}_m , we include “metal”, “wood”, “plastic”, “ceramic”, “stone”, “rubber” and “leather”.

Filtering synthesized images. Since an initial object guidance leads to a nearly-white background, we could precisely estimate the foreground object silhouette in a synthesized image. To acquire the foreground silhouette, we convert the synthesized RGB image to grayscale, and then consider pixels with values between 250 and 255 as background. Through this simple process, we could attain an accurate approximation of the foreground silhouette in most cases. After we obtain the approximated foreground silhouette, we compute IoU by comparing it with the silhouette depicted in the mask extracted from 2.5D sketch. If the value is less than $\tau = 0.95$, our data synthesis framework would filter the synthesized object image and then try to generate a new object image.

B Additional Training Details

Simulation of random occlusions. We simulate random occlusions while pre-training models. Specifically, we randomly erase an image region with 0.5 probability. The size of the erased region is randomly chosen within the range of 0.01 to 0.1 relative to a bounding box size, which is derived from an object silhouette mask. The aspect ratio of the erased region is randomly chosen within the range of 0.33 to 3.33.

Training of AtlasNet. We pre-train AtlasNet-Sphere [31] on synthetic data for 20 epochs. After the pre-training, we fine-tune the model on Pix3D [75] for 60 epochs. We train the model using Adam [38] optimizer with a learning rate of 0.0005, weight decay of 0.0001, $\beta_1 = 0.9$ and $\beta_2 = 0.999$. We use a batch size of 32. To compute Chamfer loss, we randomly sample 10K points from both predicted and ground-truth meshes. During the model training, we horizontally flip an input image with 0.5 probability.

Training of Mesh R-CNN. We adopt the default training settings (e.g., optimizer, learning rate) of Mesh R-CNN [31] used for Pix3D [75] experiments. During the model pre-training, we train voxel and mesh estimation modules on synthetic data for 20 epochs. After the model pre-training, we train all modules on Pix3D using the default settings.

C Additional Evaluation Details

C.1 Data Quality Evaluation

Evaluation of fidelity. In this paper, *fidelity* determines whether we could regard the used 3D objects as ground-truth shapes; lower fidelity indicates that the 3D objects are considered noisy 3D shape annotations. To evaluate the fidelity of each synthetic dataset, we randomly sample 500 images and annotate their object silhouette masks. We compute IoU values between the annotated silhouette masks and the silhouette masks extracted from 2.5D sketches. The lower IoU values indicate that synthesized images are paired with more noisy 3D shape annotations, which might cause less stable pre-training.

Evaluation of diversity. In this paper, *diversity* denotes the variety of visual variations in object appearances and backgrounds. To evaluate the diversity of each synthetic dataset, we measure the dissimilarity of images within a synthetic dataset (w/ LPIPS [91]) and the fraction of real data covered by synthetic data manifold (w/ improved recall [42]). In this evaluation, we only exploit chair object images to reduce the effect of substantially different shapes from different object categories. For LPIPS, we compute the value for all possible pairs within a synthetic dataset and then average values. For the recall, we compute the value using Pix3D [75] object images as real data. Following [42], we use a neighborhood size of 3 and exploit pre-trained VGG-16 [73] to extract image features.

C.2 Model Evaluation

AtlasNet [31] estimates a 3D shape in the object canonical coordinate system, whereas Mesh R-CNN [28] detects an object and then estimates its 3D shape in the camera coordinate system. Considering these differences, we use different evaluation metrics.

Evaluation of AtlasNet. Following [31, 58, 89], we compute the Chamfer distance from predicted and ground-truth meshes aligned by ICP. Specifically, we randomly sample 10K points from both aligned meshes, and then compute the Chamfer distance.

Evaluation of Mesh R-CNN. Following [28], we compute the average precision for the evaluation of this model. To calculate the average precision, we compute $F1^{0.3}$ using 10K points randomly sampled from both predicted and ground-truth meshes. $F1^{0.3}$ is the harmonic mean of precision and recall; the precision represents the fraction of predicted points within 0.3 distance from a ground-truth point, and the recall indicates the fraction of ground-truth points within 0.3 distance from a predicted point. In accordance with [28], a correct detection with $F1^{0.3} > 0.5$ is considered as a true-positive.

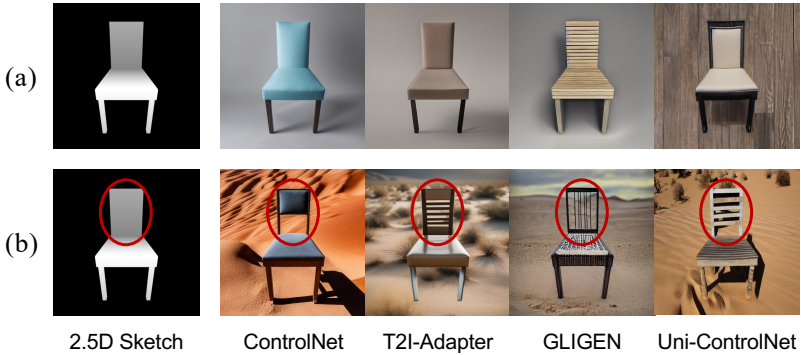


Fig. D1: Trade-off between diversity and fidelity observed from pre-trained ControlNet [90], T2I-Adapter [56], GLIGEN [45] and Uni-ControlNet [61]. (a) When we use a textual condition “a chair” and 2.5D sketch as a spatial condition, conditional generative models synthesize monotonous backgrounds in most cases. (b) A textual condition “a chair in the desert” could result in various backgrounds at the expense of violating the spatial condition. We highlight regions with red circles.

D Additional Experimental Results

Trade-off between diversity and fidelity. As shown in Fig. D1, we observed the trade-off from pre-trained conditional generative models [45, 56, 61, 90]. The observations demonstrate that such conditional generative models suffer from the diversity-fidelity trade-off issue. In this paper, we effectively tackle this issue by disentangling the synthesis process of object appearances and backgrounds. With the help of this disentangled framework, ObjectDR_{dis} could simulate a great variety of visual variations in object appearances and backgrounds while achieving high fidelity.

Extensive synthesis results. Figure D2 shows 70 images synthesized by ObjectDR_{dis} with 3D objects from ShapeNet [9]. The visualization results demonstrate that the proposed data synthesis framework actually simulates diverse visual variations in object appearances and backgrounds. We argue that such generated data would be useful for a 3D shape reconstruction model to generalize well across diverse environments. By pre-training the model on our synthesized data, it could effectively learn to capture a domain-invariant geometry prior that is consistent across different domains.

Full evaluation results of AtlasNet. In the main paper, we show AtlasNet [31] evaluation results on Pix3D [75] for the 4 object categories (bed, chair, sofa and table) since the manuscript has space constraints and we mainly utilize 3D shapes from the 4 categories. In Table D1, we show AtlasNet evaluation results for all of the 9 Pix3D object categories according to the model pre-training on synthetic data generated with ShapeNet [9] or ABO [12] objects. When we pre-train the model on ObjectDR_{dis} images, its accuracy is improved by 16.5% (0.0109 vs. 0.0127) in \mathcal{S}_1 and 18.3% (0.0224 vs. 0.0265) in \mathcal{S}_2 . Note that the pre-training with ShapeNet objects achieves higher overall improvements. This is because we utilize ShapeNet objects from all of the 55 ShapeNet object categories, whereas we only exploit ABO objects from the 4 object categories. In Table D2, we also show pre-trained only model results for all of the 9 Pix3D object categories.

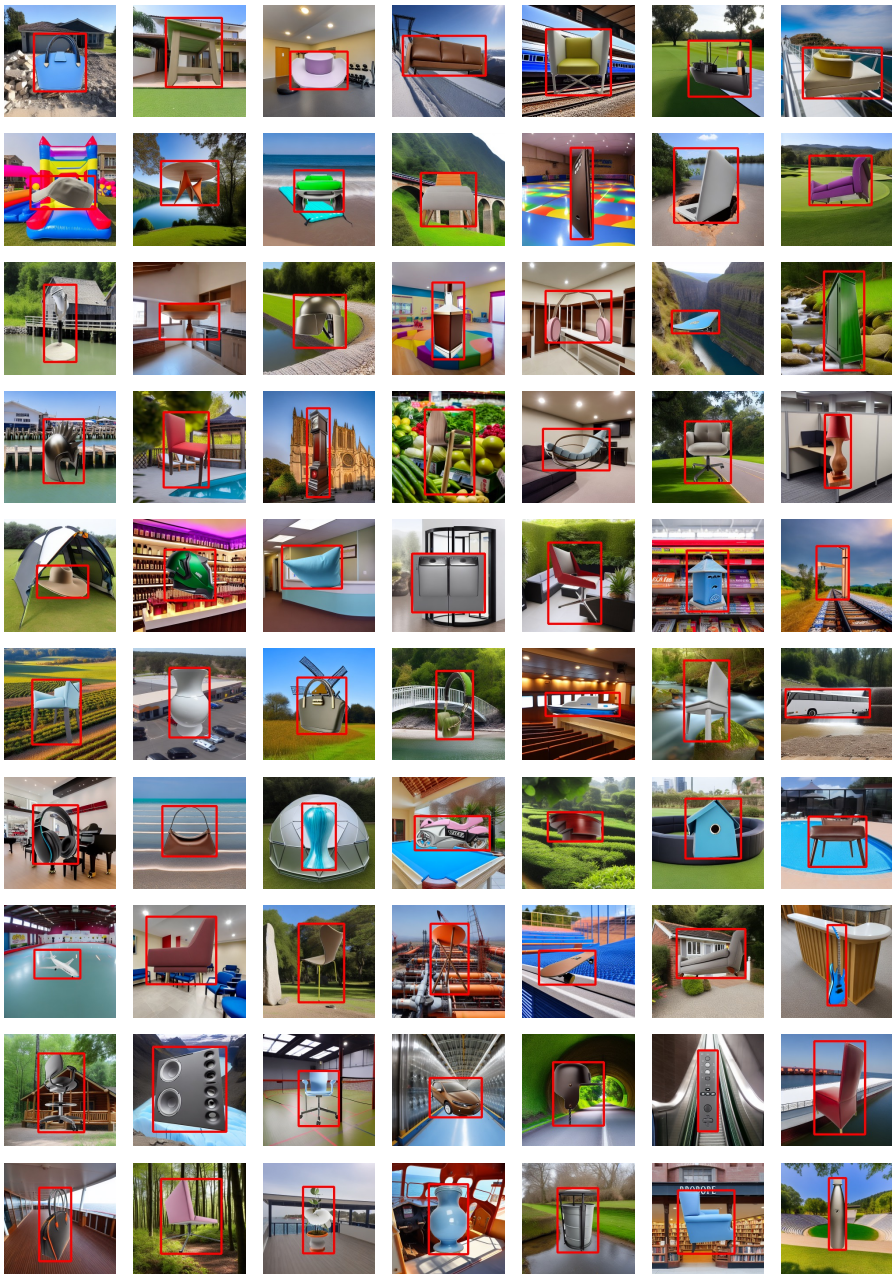


Fig. D2: Extensive synthesis results. We show 70 ObjectDR_{dis} images generated with 3D objects from ShapeNet [9]. For the purpose of better visualizations, we draw bounding boxes with red rectangles. The bounding boxes are derived from object silhouette masks.

Table D1: Evaluation of AtlasNet-Sphere [31] on Pix3D [75] \mathcal{S}_1 and \mathcal{S}_2 splits. We pre-train the 3D shape estimation model on synthetic data generated with ShapeNet [9] or ABO [12] objects, and then fine-tune the model on the train set in each split. Note that we use PyTorch3D [64] renderer to render 3D shapes from ShapeNet, and Blender [13] renderer to render 3D shapes from ABO.

Pre-training		Chamfer Distance (10^{-3}) \downarrow									
Data Synthesis		bed	bookcase	chair	desk	misc	sofa	table	tool	wardrobe	mean
\mathcal{S}_1	–	7.4	6.7	15.7	22.1	18.9	5.3	29.1	5.7	3.8	12.7
	PyTorch3D [64]	7.1	6.7	14.8	20.9	17.7	5.2	28.2	5.9	3.7	12.2
	ObjectDR	6.9	6.3	14.4	19.1	16.3	5.2	26.8	4.6	3.3	11.4
	ObjectDR_{dis}	6.5	6.3	13.7	18.6	14.7	5.0	25.8	4.2	3.4	10.9
	Blender [13]	7.0	6.4	14.5	21.5	19.2	5.2	27.2	5.5	3.7	12.2
	ObjectDR	6.8	6.4	14.0	21.3	19.0	5.1	26.7	5.6	3.7	12.1
	ObjectDR_{dis}	6.5	6.3	13.3	21.1	18.1	4.9	26.2	4.9	3.5	11.6
	–	28.9	9.1	18.5	32.9	46.8	5.7	59.5	11.3	26.1	26.5
\mathcal{S}_2	PyTorch3D [64]	27.9	9.5	17.5	28.3	43.4	5.9	55.9	10.2	23.3	24.7
	ObjectDR	26.2	8.8	17.0	28.7	44.8	5.7	52.3	9.7	21.5	23.9
	ObjectDR_{dis}	25.7	8.9	16.0	26.8	37.1	5.6	50.1	9.9	21.7	22.4
	Blender [13]	27.4	8.6	17.1	32.2	47.3	5.8	52.8	10.8	22.8	25.0
	ObjectDR	26.1	8.8	16.8	32.8	47.1	5.6	52.2	11.1	22.5	24.8
	ObjectDR_{dis}	25.6	8.5	15.9	32.7	46.5	5.6	50.3	10.7	21.8	24.2

Table D2: Ablation study on randomizing pre-training data. We pre-train AtlasNet-Sphere [31] on synthetic data generated with ShapeNet [9] objects, and then fine-tune the model on the train set in Pix3D [75] \mathcal{S}_2 . From untextured objects, we randomize their appearances and backgrounds.

Pre-training Data		Chamfer Distance (10^{-3}) \downarrow									
		bed	bookcase	chair	desk	misc	sofa	table	tool	wardrobe	mean
\mathcal{S}_2	Plain Object Shapes	28.1	9.8	17.9	28.9	48.3	5.9	56.3	11.2	24.4	25.6
	+ Random Appearances	26.4	8.9	16.9	28.2	43.6	5.7	52.6	9.6	21.8	23.7
	+ Random Backgrounds	25.7	8.9	16.0	26.8	37.1	5.6	50.1	9.9	21.7	22.4

E Discussion

E.1 Diversity-Fidelity Trade-off

This issue is attributed to the training procedure of conditional generative models (*e.g.*, ControlNet [90]). They are trained with 2.5D sketches which contain both foreground and background information. Thus, they tend to synthesize monotonous backgrounds if we use 2.5D sketches rendered from 3D objects; the sketches lack background information.

E.2 3D Shape Reconstruction in the Wild

In this paper, we aim to facilitate 3D shape reconstruction in the wild. To achieve the goal, we pre-train a 3D shape reconstruction model on our randomized data so that the model learns to capture a domain-invariant prior that is consistent across a variety of environments, improving its robustness to diverse backgrounds. To enhance its resilience against occlusions, we also simulate random occlusions during the model pre-training.

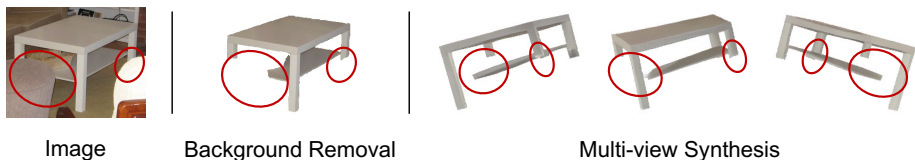


Fig. E1: Fundamental problem of the two-stage estimation approach which first removes backgrounds and then reconstructs 3D shapes from images with no backgrounds. The background removal eliminates occluded object regions, and thus multi-view synthesis cannot depict missing object parts (e.g., a table missing legs). In this visualization result, we use Wonder3D [49] for the multi-view synthesis. We highlight regions with red circles.

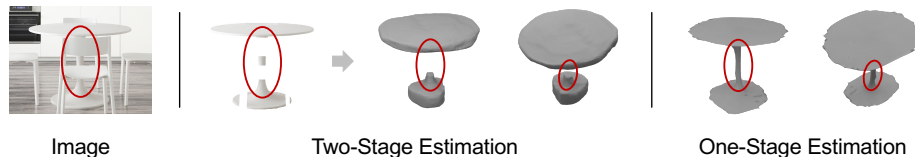


Fig. E2: Comparison of estimation approaches. The two-stage estimation approach removes backgrounds and then reconstructs 3D shapes, whereas the conventional one-stage estimation approach directly reconstructs 3D shapes. Note that the two-stage estimation is severely hindered by occlusions. In this visualization result, we use CRM [81] for the two-stage estimation and Mesh R-CNN [28] for the one-stage estimation. We highlight regions with red circles.

Unlike our approach, one might devise a two-stage estimation approach for 3D shape reconstruction in the wild: (1) remove backgrounds, and then (2) reconstruct 3D shapes from images with no backgrounds. This approach could exploit multi-view synthesis with diffusion models [47, 49, 81] which enable multi-view 3D shape reconstruction from a single image. However, this two-stage approach has a fundamental problem as shown in Fig. E1. If an object is occluded by surrounding environments, occluded object regions would be eliminated by the background removal. As a result, multi-view synthesis would fail to depict missing object parts. Furthermore, estimation errors would be accumulated during the two-stage estimation if the background removal is not perfect.

In Fig. E2, we compare 3D shape reconstruction results of the two-stage estimation approach with the conventional one-stage estimation approach. It demonstrates that the two-stage approach suffers from estimating occluded object parts, since the background removal process eliminates occluded regions. In contrast, Mesh R-CNN [28] pre-trained on our randomized data performs reliably despite the presence of occlusions.

F Ethics Considerations

Our data synthesis framework exploits 3D object collections and conditional generative models. To avoid conflicts, one should carefully follow their usage rights, licenses and permissions. Also, one should be aware that generative models might reflect biases inherent in their training data [20], and object images in the training data might also be biased [79]. Furthermore, one should keep in mind that generative models might expose their training data [6]. To avoid data privacy issue, one could leverage erasing methods [24, 57] capable of removing unwanted concepts from generative models.